Ultrasonics 96 (2019) 149–159

Contents lists available at ScienceDirect

Ultrasonics

journal homepage: www.elsevier.com/locate/ultras

Waveshape distortion of high frequency acoustic waves in gas media

H.A. Bennett[a,*], B.S. Cazzolato[a], D.M. Huang[b], A.C. Zander[a]

[a] School of Mechanical Engineering, The University of Adelaide, Australia
[b] Department of Chemistry, School of Physical Sciences, The University of Adelaide, Australia

ARTICLE INFO

Keywords:
Molecular dynamics
Acoustic wave
High frequency wave shapes

ABSTRACT

In molecular dynamics simulations of an acoustic domain excited by a sinusoidally oscillating plane acoustic source in the frequency range of hundreds of megahertz, the density and velocity perturbations adjacent to the source are observed to be non-sinusoidal in shape. This distortion in the shape of the waves is investigated using a number of simulations of frequencies in the hundred of megahertz range and velocities up to 0.50 Å/ps. The relative distortion of the wave shape is characterised by a developed nested trigonometric function. The distortion is shown to be a function of the Mach number of the acoustic source rather than the source velocity amplitude. Trends in the distortion with source amplitude and frequency indicate that distortion of the velocity and density are independent of frequency. It is shown that the density and velocity perturbation can be approximated for any sound source Mach number within the range examined using the parametrised developed equation. The developed approximation could be used to accurately simulate the influence of an oscillating plane using a stationary analytical source. This could be used to develop a hybrid molecular/continuum model that will allow lower frequency simulations. The improved understanding of the causes of the distorted high frequency waveshape could also improve the fidelity of parametric arrays.

1. Introduction

The topic of high frequency acoustic waves in the field of rarefied gas dynamics is still a very active topic, partly driven by interest in micro-electro-mechanical systems (e.g. [1]). Although a relatively simple system, there is still research into the propagation of waves in a rarefied gas between a stationary infinite plate and a parallel normally oscillating infinite plate (see [2,3]). This paper deals with such a system. Frequently, kinetic equations such as the Boltzmann equation are used to examine the evolution and propagation of acoustic waves in such systems, however, there are alternatives that can be used including Molecular Dynamics (MD), which is of interest in the current paper. MD uses interatomic force potentials to solve Newton's equations of motion applied to individual atoms in a system [4]. MD simulations can provide important insight into acoustic waves, in particular their interactions with nanomaterials, which may allow the development of nanomaterials that are more effective sound absorbers than conventional materials. However, pure MD simulations of acoustic waves can be computationally prohibitive. Hybrid molecular/continuum simulations in which a truncated MD domain is coupled to a continuum (finite-difference (FD)) domain can help to address this problem by reducing computational costs, thus allowing lower frequencies to be simulated. In such simulations, the oscillating acoustic source is modelled as an equivalent stationary (i.e. not spatially oscillating) source that functions through velocity and density manipulation of a fixed region. For such simulations to be physically accurate, the sound source must be accurately characterised, in particular by comparison with pure MD simulations to ensure any hybrid model is self-consistent with the MD portion its the domain. The characterisation of the sound source is the goal of this paper. Due to the computational expense associated with MD, this study is limited to high-frequency acoustic waves. Nevertheless, the behaviour of high-frequency sound sources is also relevant to parametric arrays [5], for which an improved understanding of waveshape could assist in maintaining fidelity of the resultant wave for higher frequency and amplitude carrier waves.

Few MD studies of acoustic waves have been carried out to date due to the prohibitive computational cost of these simulations (see [6,7]). Previous work by Yano [8] studied acoustic waves using molecular dynamics, although the focus was on qualitative discussion of wave propagation. This paper differs from the aforementioned work in that it focusses on characterising the waveshape produced in the vicinity of the source, rather than the propagation of the wave through the medium over larger distances, by a high-frequency sinusoidally oscillating wall. Although other methods, such as direct simulation Monte Carlo, could be used for the simulations, one of the intended applications is modelling the sound absorption of nanomaterials, for which a

* Corresponding author.
E-mail address: hywel.bennett@adelaide.edu.au (H.A. Bennett).

https://doi.org/10.1016/j.ultras.2019.02.001
Received 9 November 2018; Received in revised form 31 January 2019; Accepted 4 February 2019
Available online 05 February 2019
0041-624X/

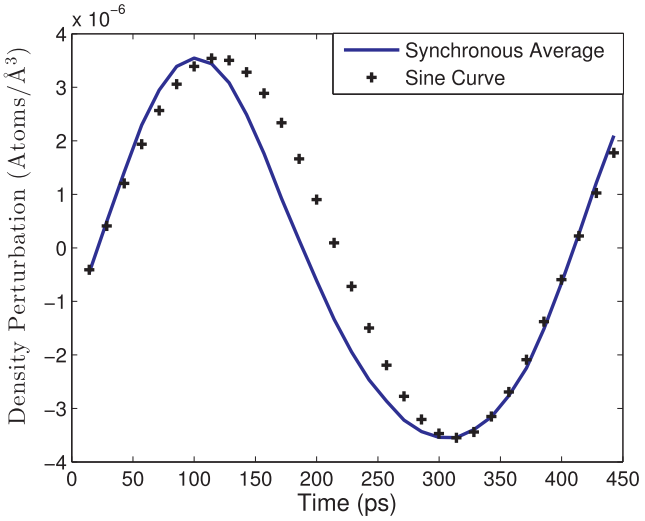

Fig. 1. The synchronous average of the density perturbation at 2570 MHz and a source velocity of 0.50 Å/ps in a domain 12000 Å in length.

comprehensive review has determined that MD is the most suitable method (see [6,9]), due to the ability to model the nanomaterial itself including structural vibrations, gas-nanomaterial interactions and the bi-directional heat transfer that occurs between the gas and nanomaterial, in addition to being able to model compressible media and acoustic waves. In such simulations, the waveshape generated by the sound source is an important consideration. This also applies to techniques that use an analytical expression to describe the sound source, or coupling techniques in which an accurate source description is required; in either case an accurate representation of the sound source is necessary.

In the current work it has been observed via MD simulations that when using a sinusoidally oscillating plane as a sound source at extremely high frequencies the temporal shape of the wave will deviate from a perfect sinusoid at a short distance from the source (Fig. 1).

Furthermore, the change in shape from a sinusoid is not limited to the steepening often observed in nonlinear acoustics [10], as it also features a change in the width of the peak and trough, which does not appear to have been discussed in acoustics literature previously. Due to the distorted waveshape being previously undocumented, the investigation of the distorted waveshape in this paper includes its documentation, theoretical analysis and parameterisation. The objective of this paper is to characterise the observed distortion and determine the main factors causing such a waveshape. Additionally, this paper investigates the dependence of the distorted waveshape on the acoustic frequency and oscillating source amplitude. The results are parameterised to facilitate their application to an equivalent stationary source for modelling purposes.

The paper is structured such that following the Model Description in Section 2, the Methodology (Section 3) discusses the use of Synchronous Averaging to remove noise from the waveshape data and the construction of a modified oscillatory curve which facilitates assessment of the distortion of the waveshapes. These techniques are applied in the Results and Analysis section (Section 4) to the piston force, velocity wave and density wave, in sequence. This order leads to the discussion of the observable in order of their level of distortion. The analysis demonstrates that a pseudo-Doppler effect is a major contributor to the distortion observed and culminates in a parameterisation of the distortion which is dependent on the sound speed normalised piston velocity.

2. Model description

The model examined in this paper was based on the work of Ayub et al. [11], which investigated the acoustic absorption in a monatomic gas using MD. However, the dimensions of the system and interaction cutoff distances have been altered, and the atomistic sound source has been replaced with an analytical function. The system consisted of an argon gas medium excited by an acoustic wave produced by an oscillating plane. The MD domain was a three-dimensional cuboidal box. All simulations were performed using the MD software LAMMPS [12].

The domain size used for the simulations was 1565 Å × 1565 Å × 12000 Å. The x and y dimensions were greater than those found in other acoustic-MD studies [11] to ensure there were a sufficient number of atoms for averaging, while also maintaining a manageable computational load. The domain was populated with argon gas atoms using a 53 Å face-centred cubic lattice, then equilibrated for 200 million timesteps at 273 K, to be consistent with [11] and ensure a steady-state was achieved. This creates a system with a density of 2.67×10^{-5} atoms/Å^3 (1.8 kg m^{-3}), and a mean free path of 729 Å.

The interatomic collisions for the argon gas were modelled using a Weeks-Chandler-Andersen (WCA) potential [13] and Lennard-Jones (LJ) parameters from [11]. The WCA potential models purely-repulsive elastic collisions consistent with monatomic gas physics. WCA is also a good approximation of a hard-sphere, but can be more readily modelled due to being continuous and differentiable. A Lennard-Jones 9-3 wall [14] was located at the near end of the domain in the z-direction, and was oscillated sinusoidally in the z-direction to simulate a sound source. As the position of the piston was kinematically defined, and its trajectory would not be changed regardless of the force exerted on the analytical wall, the piston could be considered an infinite impedance acoustic source. The LJ 9-3 wall potential was selected since it is analogous to a semi-infinite solid and is considered to better replicate a real sound source, which would consist of a moving diaphragm several orders of magnitude thicker than the size of the simulated domain. To make the wall purely repulsive, the cutoff distance for the potential was selected to match the minimum of the potential, resulting in a potential equivalent to the WCA potential [13]. The trajectory of the sound source was defined by a sinusoid at the desired frequency and velocity amplitude. Frequencies of 321, 643, 1285 and 2570 MHz were selected in order to span frequencies including that modelled by Ayub [6], with the lowest frequency corresponding to an acoustic wavelength shorter than the domain length (as discussed further in Section S1 of the supplementary material document). The Knudsen number, defined as the excitation frequency divided by the mean collision frequency, can therefore be seen to range between approximately 0.06 and 0.5, indicating transition flow, between continuum and molecular flow. Source velocity amplitudes of 0.031, 0.062, 0.124, 0.25 and 0.50 Å/ps were applied for each frequency, allowing the relationship between the source velocity amplitude and the waveshape to be analysed. The maximum velocity is consistent with that used by [11,2] and though it is approximately 15% of the speed of sound it was seen as significant but not excessive given the attenuation observed at such high frequencies. Particular care should be given when considering the frequency–amplitude combinations, leading to very small piston displacements, such as those with very high frequencies and very low velocity amplitudes, since they may not lead to accurate results (as discussed further in Section S1 of the supplementary material document).

An LJ 12-6 wall was positioned at the far end of the domain in the z-direction, acting as a reflective wall. This wall was also purely repulsive, modelled by a WCA potential [13]. The remaining boundaries in the x and y directions were periodic, as this avoids boundary layer formation along these domain edges and characterised the flow as being free rather than flow within a nanochannel or micropore.

During the simulation a Nosé-Hoover thermostat was applied only to the velocity components perpendicular to the direction of wave

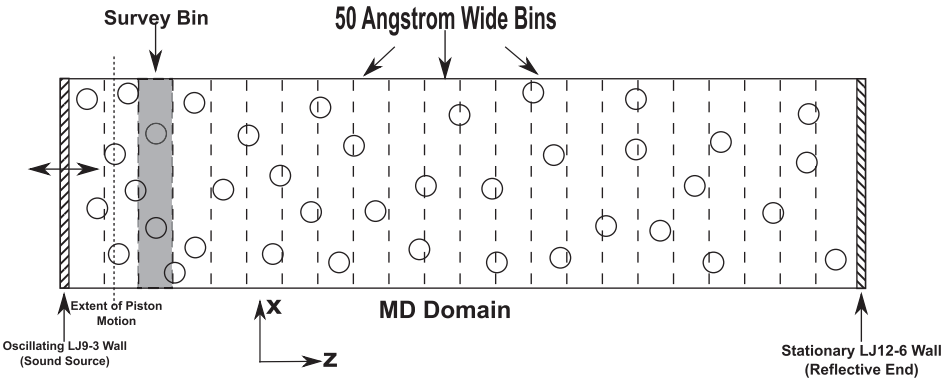

Fig. 2. A schematic of the system and positioning of survey bin (not to scale).

propagation (x and y) and had a damping time matching the period of the acoustic wave. This avoided the thermostat interfering with the formation and propagation of the acoustic wave, and permitted the temperature oscillation produced by the wave, while preventing systematic temperature drift [6].

Timesteps of 10 fs were used in the simulations, as previous simulations had demonstrated that the gas interactions were sufficiently infrequent to make this timestep permissible.

Simulations varying the density and temperature of the system were also undertaken to determine the influence of diffusion coefficients and wavespeeds on the distortion of the waveshape. These results are discussed in detail in Section S2 of the supplementary material document.

The domain was subdivided along the z-direction into slices 50 Å wide (see Fig. 2), referred to as bins, to allow the variation in parameters such as velocity, density and temperature to be monitored with respect to distance from the acoustic source. A bin width of 50 Å was selected as it balances the desire to reduce the stochastic variation by including a large number of atoms against the need for spatial resolution. On average, a bin in this arrangement contained approximately 3000 atoms and for the highest frequency investigated spanned approximately 1/30th of a wavelength, and less at lower frequencies.

3. Methodology

Due to the randomness inherent in MD simulations it was necessary to apply a synchronous averaging technique in order to extract the underlying waveshape, as described in Section 3.1. After averaging, the extracted waveshape was described using a developed oscillatory curve (Section 3.2), with the parameters being derived through curve fitting. The trends in the parameters across different simulations were used to clarify the causes of the waveshape distortion. The relationship between the parameters and the acoustic source was also parameterised (see Section 3.3), both to support the analysis of the underlying causes of wave distortion and to allow the appropriate curve function to be determined for a source with arbitrary frequency and amplitude. This function characterises the wave and is necessary for implementing an equivalent stationary source.

3.1. Synchronous averaging

Synchronous averaging was used to remove the noise from the MD output and extract the waveform. Before averaging, the data must first be extracted from the simulation in an appropriate form.

The 50 Å bins were used to calculate the average z-velocity and density, the acoustic parameters used to describe the plane wave. To reduce the influence of random fluctuations, block averaging was also used temporally, with samples being taken every few timesteps and averaged every 14.28 ps, the time taken for a wave to propagate the bin width. For the selected averaging frequency, it can be shown that even at the highest source frequency examined a reasonable number of samples were calculated for each wave period, allowing appropriate representation of the wave. As a guide, the preferred averaging frequency approximates or slightly underestimates the time taken for sound to travel the width of the bin, since this prevents over sampling, which would be inefficient, and the bin width is at most 5% of the wavelength. The series of averages for a specific bin can then be taken to be the signal of interest, with signal analysis techniques providing insight into the wave passing through the bin, with respect to both density and velocity.

Density was selected as an acoustic parameter in preference to pressure as it can be more easily calculated in the MD simulation. Furthermore, for future development of a hybrid molecular/continuum (MD-FD) model, for which modification and control of the wave is desired, the density can be manipulated more readily than the pressure. Manipulation of the pressure would necessitate density alteration; hence it is also more efficient to work with the density directly in MD simulations.

To analyse the sound source, the parameters were observed at a specific bin. The location of the observation bin is particularly important, as it is necessary that the bin be far enough from the source to avoid near field effects, while being as close to the source as possible in order to observe the source signal with as little attenuation as possible. Fig. 3 demonstrates the extreme attenuation in the system, which also indicates that any reflected wave component will be negligible near the source. Thus, the waveshape seen at the observation bin relates only to the propagating wave, due to the lack of a reflected wave component. The visible noise in Fig. 3b), which is the block averaged velocity at the bin, demonstrates the need for synchronous averaging even for a high amplitude case with a greater signal-to-noise ratio.

The extent of the near field was determined by finding the closest bin to the source that was beyond the fully extended position for the oscillating wall and for which the centreline of the z-direction velocity waveform was within 0.007 Å/ps of zero (which avoids complications due to the combination of both the skewed wave shape and density variations in time). This bin is henceforth referred to as the 'survey bin'. The position of the survey bin within the simulation domain is illustrated generally in Fig. 2 and for a particular case in Fig. 3.

The signal for the wave velocity and density was obtained from the survey bin, while the wall force was directly calculated from the interactions. Synchronous averaging was performed in post-processing by extracting a number of segments of the signal (at least 100 were used in each case, more were used when feasible), each containing a synchronised period of the signal, and averaging these segments to determine an average signal (see example in Section S3 of the supplementary material document). For low signal-to-noise ratio cases a lowpass filter was also used to remove noise from the signal prior to synchronous averaging (further details in Section S3 of the supplementary material document), however, as it could attenuate frequencies of interest using

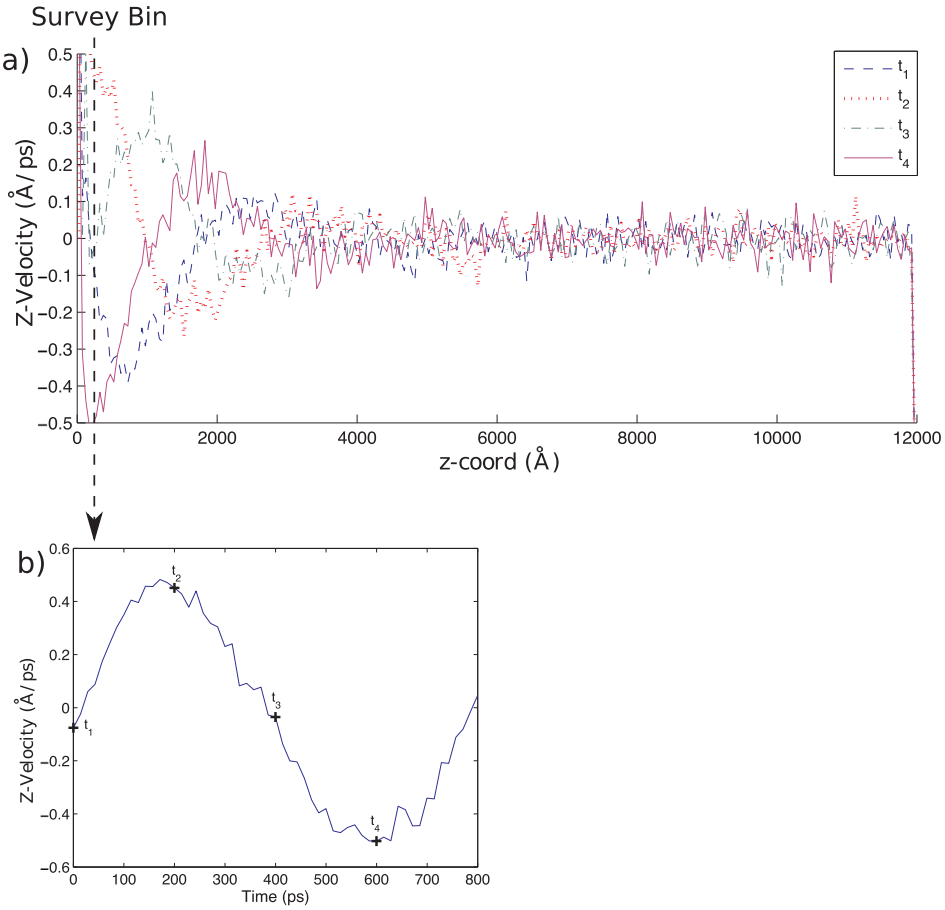

Fig. 3. The velocity from a 1285 MHz 0.5 Å/ps case, (a) over the whole domain for four points in time, t_1, t_2, t_3, t_4, and (b) observed at the survey bin spanning $t_1 - t_4$.

the filter was avoided as far as practical.

3.2. Modified oscillatory curve

Since the piston acts as an infinite impedance acoustic source and oscillates sinusoidally, it would be expected that the density fluctuation and velocity of the acoustic wave produced would be sinusoidal. However, as seen in Fig. 1, which displays the synchronous averaged density, the waveform for a 2.57 GHz 0.50 Å/ps source is not sinusoidal. Futhermore, Fig. 3 demonstrates the reflected wave is negligible at the survey bin and, hence, the shape does not result from the superposition of two sinusoidal curves. This indicates the need to develop an oscillatory function that characterises the observed waveshape.

For the desired purposes it is necessary that the function be general, but avoid complexity as far a possible. Thus, using a generic sinusoid as a foundation, alterations have been limited to trigonometric functions. The features observed in the distorted wave that need to be reproduced by the oscillatory function are the change in the width of the peak and trough, and relative position of the peak and trough (which are no longer half a period apart). This is possible through modifying the time function. However, the function must maintain the same periodicity as the generic sinusoid and be smoothly continuous. This is achieved through selecting continuous trigonometric functions with identical periods to the piston oscillation. A nested squared sine increases the rate of progress through time during the first half of the period, and slows the progress in the second half, leading to the narrow peak and wide trough desired. The positive first half-period of a nested sine function shifts the peak of the enclosing function earlier, while the negative last half-period delays the minima, allowing control of the relative position of the peak and trough. Thus, a generalised equation for curve fitting which allows straightforward comparison between the shapes of the different distorted sinusoidal curves is

$$O(\omega, \psi, \chi) = A\sin(\omega t + \psi\sin^2(\frac{\omega t}{2}) + \chi\sin(\omega t)) \quad (1)$$

where A is the (bilateral) amplitude of the wave, ω is the frequency, t is the time, and ψ and χ are nondimensional parameters used for comparing the shapes of different waves. O refers to the relevant observable being investigated, such as the mean gas particle velocity in the propagation direction, the density perturbation and the normal force experienced by the acoustic source. As the frequency ω of both nested sinusoidal functions is consistent with the frequency of the enclosing function without those nested functions, the frequency of Eq. (1) is ω. The ψ parameter impacts the relative width of the peak and trough, and will be referred to as the 'width term'. The χ parameter, referred to henceforth as the 'steepening term', controls the steepening of the function, shifting the position of the peak and trough closer to or further from the half period, leading to a steeper decline or incline, respectively. The width and steepening terms are henceforth referred to collectively as the waveshape parameters or curve parameters. The influence of the waveshape parameters is demonstrated in Fig. 4 using arbitrary values for the width and steepening terms and a frequency of 1 rad/ps.

The combination of non-zero ψ and χ values allows a variety of distorted sinusoid shapes to be produced with varying peak and trough widths and positions. ψ and χ have limits of $\pi/2$ and $\pi/4$, respectively, to ensure that only one oscillation is present per period. All values found via curve fitting in this paper are much smaller than these limits.

To perform curve fitting, the synchronous averaged waveform was firstly centred about zero on the amplitude axis to have matching maximum and minimum amplitudes, as Eq. (1) varies between $\pm A$. A

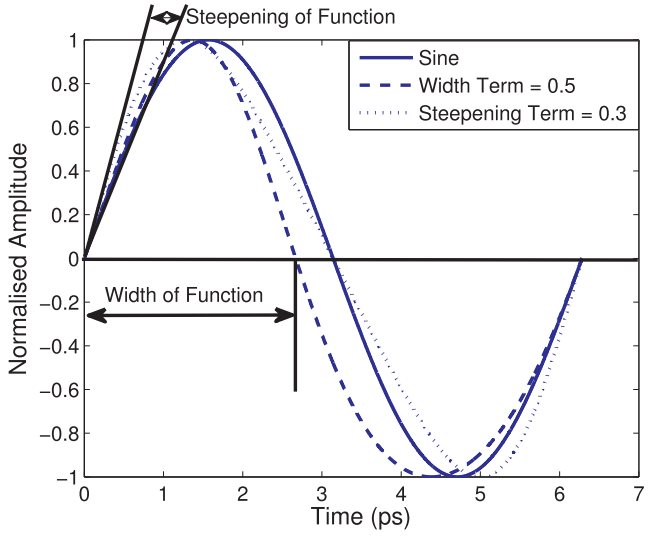

Fig. 4. The shape impact of the width and steepening terms ψ and χ in Eq. (1) compared with a sine curve with frequency of 1 rad/ps.

least mean squares method was used for curve fitting to determine the ψ and χ values. Fig. 5 displays the curve fitting obtained for the density synchronous average previously shown in Fig. 1. The curve fits from which the data used in the body of this paper were obtained are included in the supplementary material document.

3.3. Parameterisation

A parameterisation of the width and steepening terms can be achieved through curve fitting based on one of the source variables, such as the velocity amplitude (Mach number). It is generally observed in experimental cases at audible frequencies that there is minimal distortion of the waveshape when the wave amplitude is sufficiently low. Theoretically, it is clear that the wave should tend towards a pure sinusoid as the source amplitude tends towards zero. Thus parameterisations were constructed such that the waveshape parameters, ψ and χ, generalised as $\mathscr{R}$ henceforth, would be zero when the source amplitude is zero. In cases where the trend appeared to be linear a fit to

$$\mathscr{R} = mM \tag{2}$$

was used, while higher order trends were fitted using

$$\mathscr{R} = nM^p \tag{3}$$

as both of these equations satisfy the zero intercept requirement. Here, M is the source velocity amplitude as the Mach number, m is the slope coefficient, n is the amplitude coefficient and p is the exponent. Due to both the parameters and the Mach number being dimensionless m, n and p are also dimensionless. A least mean squares method was used for the fitting of the parameterised curves, obtaining the m or n and p values which best approximated the parameter dependence on the source amplitude.

4. Results and analysis

To characterise the source and investigate the factors that contribute to the observed nonlinear waveshape phenomenon, the piston force and survey bin velocity and density were analysed. Preliminary simulations, presented in the supplementary material document, were used to determine which variables could be excluded from further investigation as not directly related to the distortion of the waveshape. Simulations varying the system density demonstrated that the diffusion coefficient of the gas was not an influential factor on the waveshape. Altering the system temperature revealed that the curve parameters, ψ and χ, depend on the normalised source velocity amplitude (Mach number) rather than the absolute source velocity amplitude. As such, further parameterisations will use the Mach number rather than the source velocity in Å/ps.

The analysis of the results begins by discussing the piston force, as it is distinct from the velocity and density, since the piston moves,

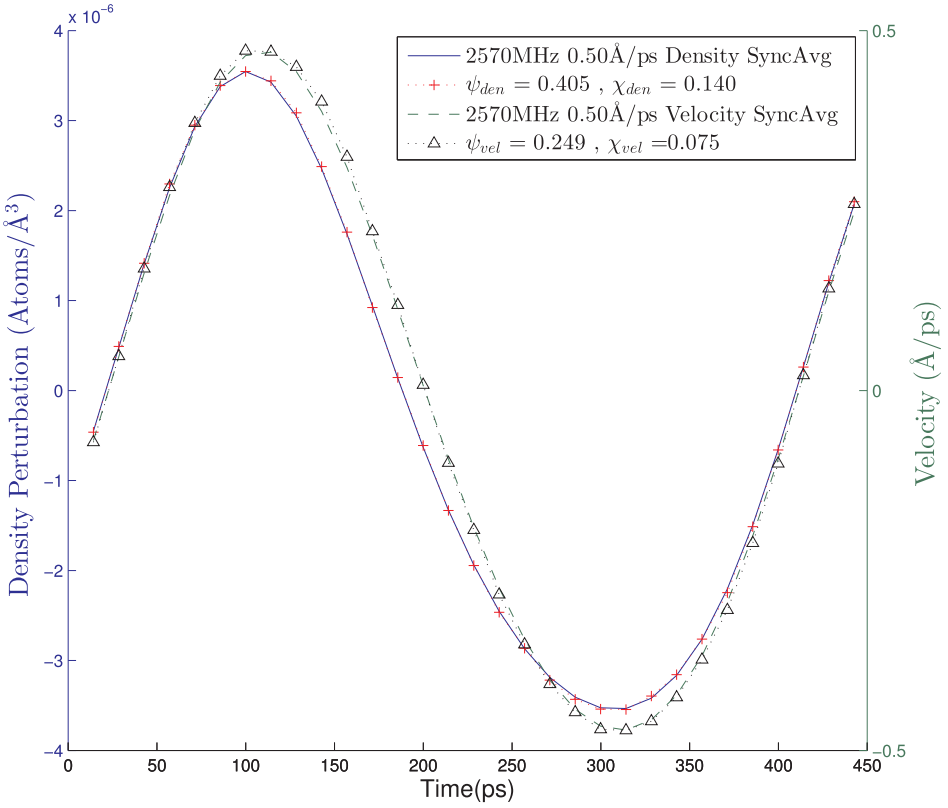

Fig. 5. Comparison of the fit curve against the synchronous average of a simulation with 12000 Å domain length and 2570 MHz, 0.50 Å/ps source for both density and velocity. For density, $\psi = 0.405$ and $\chi = 0.140$, and for velocity $\psi = 0.249$ and $\chi = 0.075$, as obtained from the least squares fit.

whereas the survey bin is fixed in space. Furthermore, as the piston is the source of the wave and the survey bin is downstream, this analysis assists with understanding the evolution of the wave. The velocity is then discussed, since it does not depend on the piston force, allowing some analysis in isolation. Finally, the density is discussed with the analysis being informed by that of the two preceding observables.

4.1. Piston force

The force normal to the oscillating plane was calculated from the interactions between the gas atoms and the wall. The piston experiences a force even when stationary due to interactions with the thermostatted gas. At the macro-scale this would be considered the gas pressure. The force perturbation changes based on the number of interactions and their magnitude. In low source Mach number conditions, it is reasonable to assume that the perturbation of the force acting on a moving wall is proportional to the velocity of the wall, based on the classical acoustics relationship between pressure perturbation and velocity. Collisions occur between the wall and neighbouring atoms with a z-velocity lower than that of the wall. This means the number of collisions is based on the z-velocity distribution, which is normally distributed about zero with standard deviation dependent on the temperature ($\sigma = \sqrt{kT/m}$), according to the Maxwellian distribution (as seen in Fig. 6).

For velocities much smaller than the standard deviation, the variations in the integral of the distribution about zero can be approximated as being linear with respect to the velocity. However, given the distorted waveshape observed, this clearly does not apply in this case. The assumption appears to break down as the velocity of the wall increases, and thus requires further investigation.

4.1.1. Force data

The force curve data for the width parameter, shown in Figs. 7 and 8 including the uncertainty in the measurements, demonstrates the width parameter clearly has a strong dependence on the source Mach number. The relatively flat response in relation to frequency emphasises this.

The steepening term values for the force curves (Figs. 9 and 10) are small, both relative to the width terms of the force curves and the steepening terms of the velocity and density curves (as will be seen in Sections 4.2.1 and 4.3.1). As the error bars in Figs. 9 and 10 all enclose zero it may be suggested that the noise floor has been reached and thus the steepening of the force curve is negligible. Thus, steepening is not strongly associated with the generation of the wave at the source.

4.1.2. Force analysis

Given that the force curve features a non-negligible width term in the cases plotted in Figs. 7 and 8, it is evident that the force perturbation is not solely a function of the instantaneous velocity of the piston. The non-linear shape of the force curve must therefore be related to another factor that influences the interactions of the fluid with the piston. A key assumption that exists alongside the velocity assumption is that the density of the region adjacent the piston is constant for any two instances, leading to the interactions scaling linearly with the instantaneous velocity. However, at elevated piston velocities, the density of the region adjacent to the piston deviates from the steady-state density, to the extent that there is a noticeable change in the number of interactions with the piston beyond the expected velocity relationship. The density of the region at an instant depends on

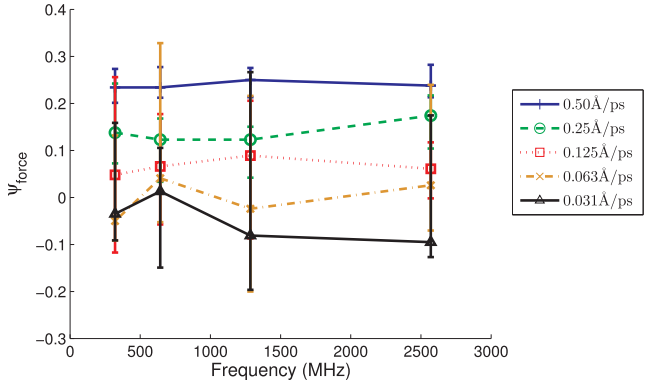

Fig. 7. The width term of the force curve, ψ_{force}, with error bars of two standard errors, as a function of frequency for different source amplitudes. (Colour available online).

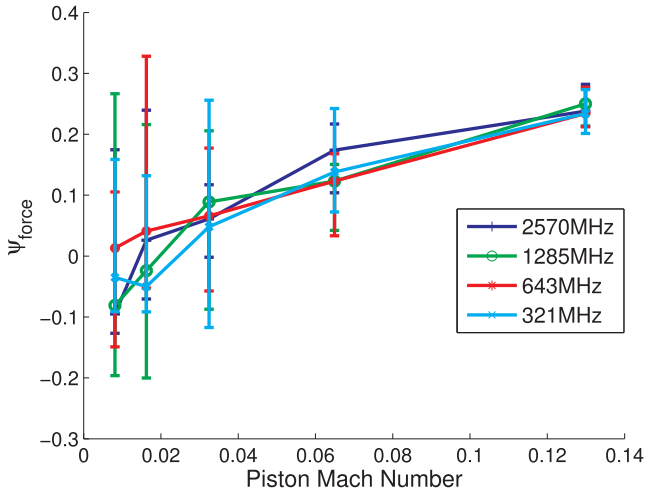

Fig. 8. The width term of the force curve, ψ_{force}, with error bars of two standard errors, for different frequencies as a function of source Mach number based on the source velocity amplitude. (Colour available online).

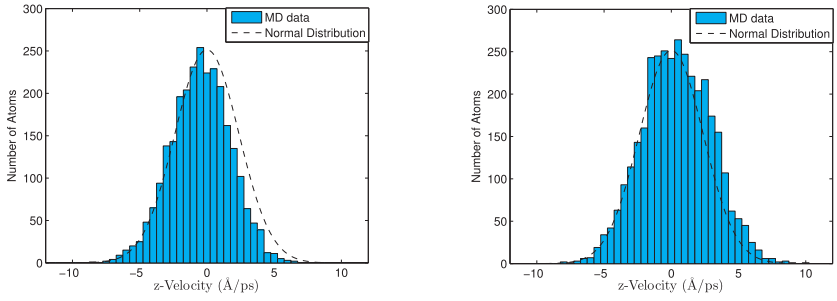

(a) Distribution example observed in a bin during wave rarefaction.

(b) Distribution example observed in a bin during wave compression.

Fig. 6. The z-velocity distribution for a region adjacent to the piston is approximately normally distributed, as expected.

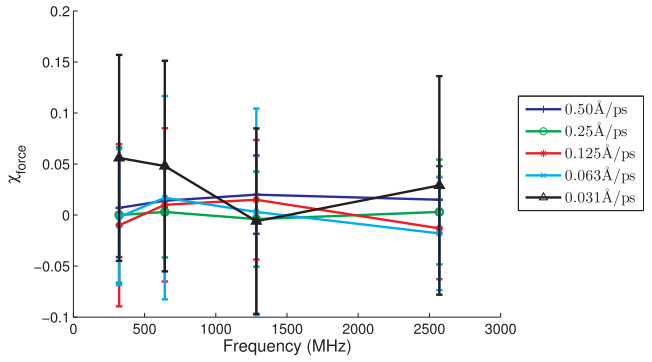

Fig. 9. The steepening term of the force curve, χ_{force}, with error bars of two standard errors, as a function of frequency for different source amplitudes. (Colour available online).

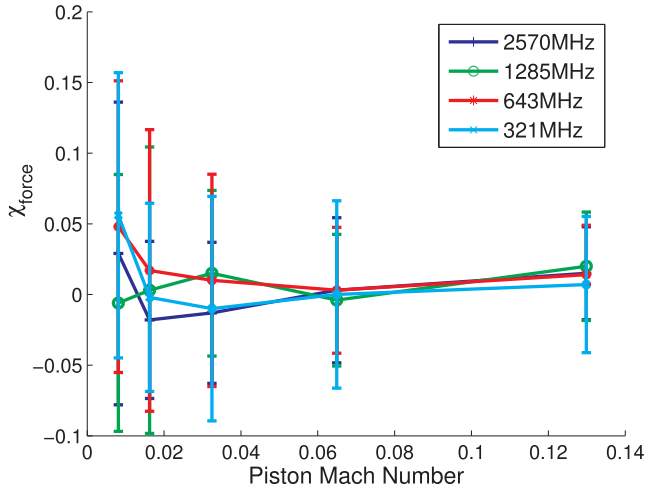

Fig. 10. The steepening term of the force curve, χ_{force}, with error bars of two standard errors, as a function of the normalised source velocity amplitude (Mach number) for different frequencies. (Colour available online).

the motion of the piston prior to that instant, with the formation of a compression or rarefaction in front of the piston. Thus memory effects are relevant to the distortion of the force waveshape. As the density adjacent the piston becomes related to the preceding piston velocity, rather than being constant, the force ceases to be linearly related to the velocity. The compounded relationship results in the sharper peak observed in the force curve. This is further enhanced by the width of the velocity distribution scaling with the root of the temperature, which increases and decreases due to the compression and rarefaction of the gas region, leading to more energetic interactions.

During the retraction of the piston, the number of interactions decreases since a collision requires an atom to have a velocity that exceeds the retraction rate of the piston, the probability of which is based on the velocity distribution. This compounds with the changing density of the region adjacent to the piston to produce the widened trough observed as the non-negligible ψ values in Fig. 8.

4.2. Velocity wave

Unlike the piston force, the measurement of which follows the motion of the piston, the velocity results were observed from the stationary survey bin shown in Fig. 2. This replicates the use of a fixed-position velocity-microphone in an acoustics experiment. The velocity is of particular interest as the mean gas velocity at the piston surface will necessarily match the surface velocity due to the Dirichlet boundary condition, which means that the accumulation and memory

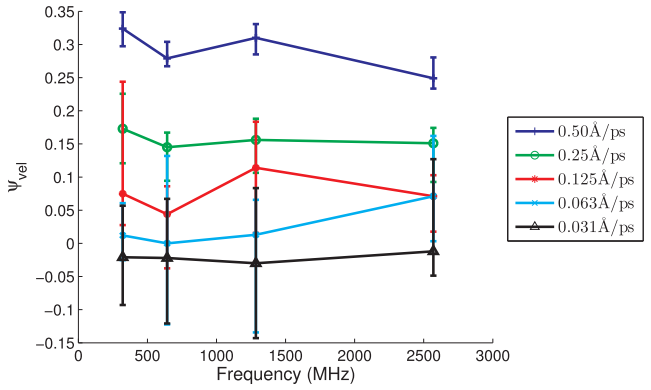

Fig. 11. The width terms of the velocity curves, ψ_{vel}, with error bars of two standard errors, as a function of frequency for different source velocity amplitudes. (Colour available online).

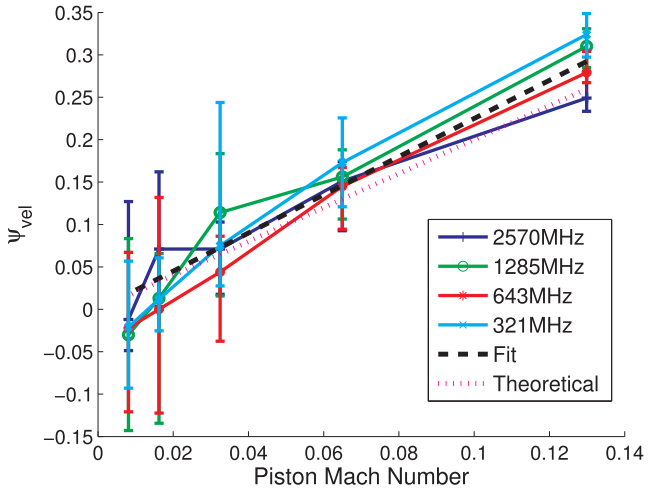

Fig. 12. The width terms of the velocity curves, ψ_{vel}, with error bars of two standard errors, as a function of the normalised velocity amplitude (Mach number) for different frequencies. A curve of best fit to the data using Eq. (2) and theoretical trend using Eq. (9) are also applied. (Colour available online).

effects that are of concern for the force and density are not present for the velocity case.

4.2.1. Velocity data

Figs. 11 and 12 show that the velocity wave width term depends linearly on the source Mach number but not on frequency. Most of the curves of Fig. 11 are relatively flat, suggesting negligible frequency dependence, while the curves in Fig. 12 have a visible slope and are clustered tightly together.

Unlike the force data, steepening of the velocity wave is evident from Figs. 13 and 14, with a more pronounced trend compared with the flat response visible in Fig. 10.

For the 0.031 Å/ps 2570 MHz source case, the steepening term for the velocity curve was found to be several times greater than that for any other frequency. This is due to the displacement of the piston being much smaller than the mean free path in this case. This is discussed in detail in Section S1 of the supplementary material document.

4.2.2. Velocity analysis

It is well established that the normal velocity component of a small gas region adjacent to a wall will match the normal velocity of the wall. However, from the MD simulation results the velocity wave at the survey bin was not perfectly sinusoidal, despite the sinusoidal motion of the piston. This distorted shape was found to originate from a propagation delay that depended on the source position, analogous to a

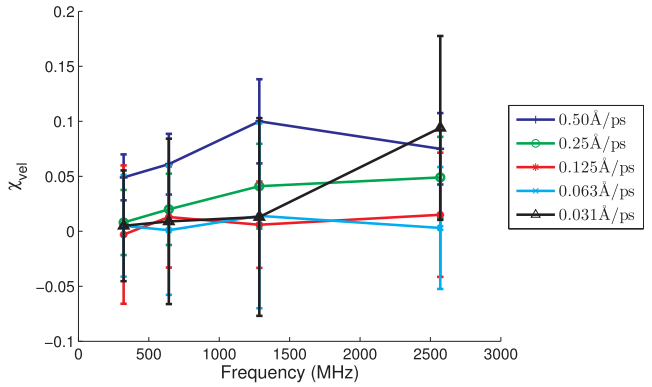

Fig. 13. The steepening terms of the velocity curves, χ_{vel}, with error bars of two standard errors, as a function of frequency for different source amplitudes. (Colour available online).

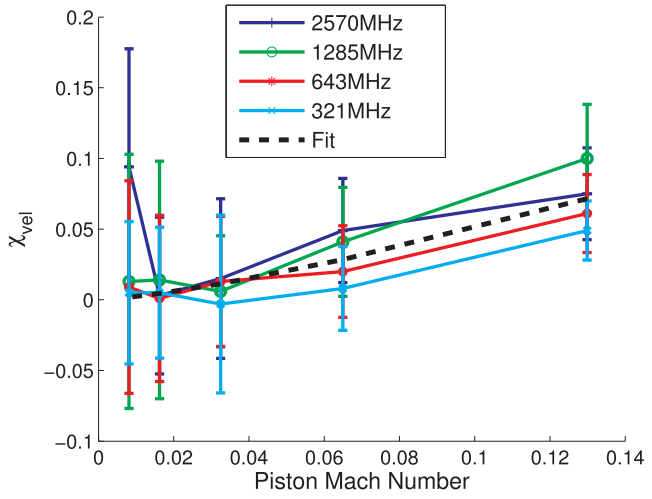

Fig. 14. The steepening terms of the velocity curves, χ_{vel}, with error bars of two standard errors, as a function of the normalised source velocity amplitude (Mach number) for different frequencies. A curve of best fit using Eq. (3) is also applied. (Colour available online).

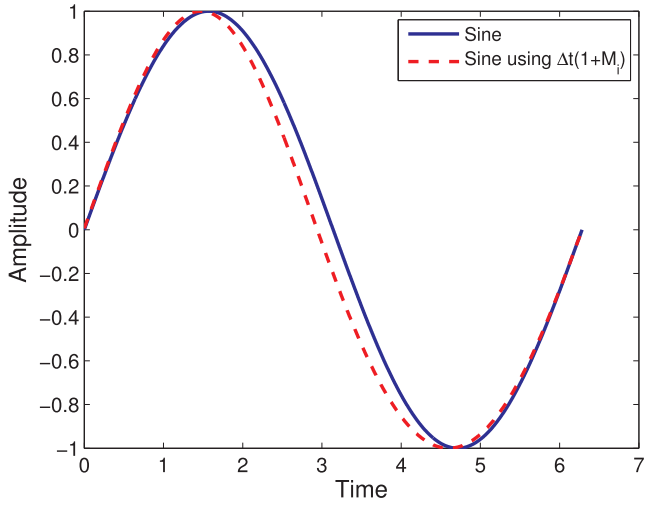

Fig. 15. Comparison of a sinusoid with and without a nonuniform time grid following Eq. (5) for a source with $M = 0.1$.

Doppler shift. The time taken for a wavefront developed by the moving wall to reach the survey bin will vary based on the position of the wall from the survey bin. As the piston undergoes motion the propagation delay of the wave changes from one moment to the next, compressing the timing when moving towards the survey bin and stretching the timing when moving away. This leads to the positive part of the velocity wave being compressed in time and the negative values being stretched, leading to the sharper peak and wider trough. This is equivalent to remapping the sine wave onto a non-uniform time grid, for which the spacing between adjacent time values depends on the Mach number of the source when the wave front was generated. Due to the velocity changing with the same frequency as the wave, the frequency definition normally applied for a Doppler shift is not appropriate. Instead we have used the time dilation/compression definition, in which the relationship between the observed (obs) and the source (src) timestep (Δt) for a sound source travelling at Mach number (velocity) M is

$$\Delta t_{obs} = \Delta t_{src}(1 + M), \tag{4}$$

noting that M will be negative when the source is travelling in the opposite direction to the propagation of the wave. The observed timestep here indicates how much of the source signal is compressed (or dilated) into a timestep when viewed at a stationary observation point. For example, a Mach number of 0.1 would lead to a stationary bin observing 1.1 timesteps worth of source signal in a single timestep. From this we can consider a running series through time such that for a timestep i, the 'new' remapped time for the sinusoidally oscillating source will be

$$t_{new(i)} = t_{new(i-1)} + \Delta t_{src}(1 + M_i), \tag{5}$$

where

$$M_i = M\sin(\omega t_i). \tag{6}$$

The curve formed through applying Eq. (5) (see Fig. 15) resembles the shape of the distorted velocity wave to the extent that the width of the peak and trough have changed.

In fact, by combining Eqs. (4) and (6) and integrating to remove the discretisation, the time transformation caused by the motion of the piston is seen to be

$$t_{obs} = t_{src} + \frac{2M}{\omega}\sin^2\left(\frac{\omega t_{src}}{2}\right), \tag{7}$$

which when substituted into the ordinary oscillatory equation

$$\mathcal{W} = \sin(\omega t_{obs}), \tag{8}$$

results in

$$\mathcal{W} = \sin\left(\omega t_{src} + 2M\sin^2\left(\frac{\omega t_{src}}{2}\right)\right), \tag{9}$$

which is essentially the modified oscillatory equation with $\psi = 2M$ and no χ term.

The change in the time grid is not expected to be representative of the steepening seen in simulations, as this is acknowledged to be largely from propagational effects, explaining the absence of the χ term. This pseudo-Doppler effect explains some of the distortion observed at the survey bin and validates the construction of Eq. (1) to contain a squared sine term. Similarly, a time transformation can be found for the steepening of the function.

It has been established that steepening develops due to the discrepancy between the propagation speed of the peak and trough of a wave. Ordinarily, this would not warrant investigation when the inquiry is focussed on the acoustic source, but due to the notable displacement of the piston, steepening cannot simply be neglected as some steepening could occur before the wave has left the source region. It has been established that the speed of sound in an ideal gas is proportional to the root of the absolute temperature [15]. This leads to the more energetic, higher temperature peaks of the wave propagating more quickly than the less energetic, lower temperature troughs. Cursory inspection, demonstrated in Section S5 of the Supplementary Materials document, showed that the amplitude of the mean temperature

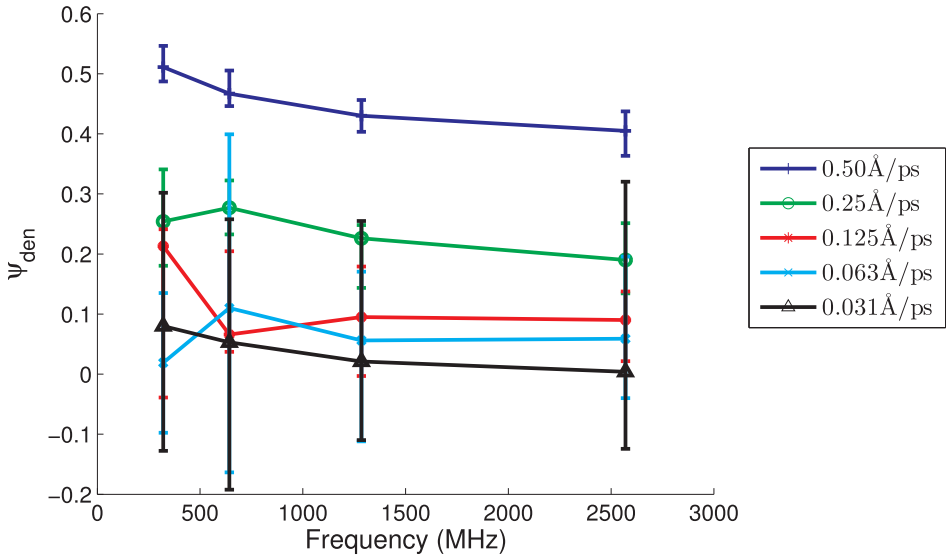

Fig. 16. The width term of the density curve, ψ_{den}, with error bars of two standard errors, as a function of frequency for different source amplitudes. (Colour available online).

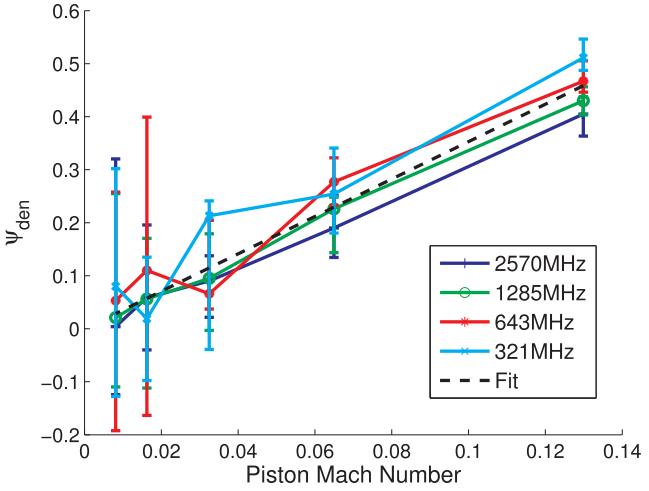

Fig. 17. The width term of the density curve, ψ_{den}, with error bars of two standard errors, as a function of the normalised source velocity amplitude (Mach number) for different frequencies. A curve of best fit using Eq. (2) also applied. (Colour available online).

variation (determined through synchronous averaging) scaled linearly with the source velocity with slope r, such that the temperature change could be approximated as rM. Thus as the speed of sound, c, is related to the local temperature by

$$c_i = c_0\sqrt{\frac{T_i}{T_0}} = c_0\sqrt{1+\frac{\Delta T}{T_0}}, \tag{10}$$

with subscript 0 referring to the reference condition, and subscript i referring to the wave section produced at the piston at time i, the change in sound speed is related to the Mach number by

$$\Delta c_i = c_0\left(\sqrt{1+\frac{rM_i}{T_0}}-1\right). \tag{11}$$

Combining with Eq. (6), for sufficiently small temperature changes, this equation can be approximated to

$$\Delta c = c_0\left(\sqrt{1+\frac{rM}{T_0}}-1\right)\sin(\omega t_{\text{src}}). \tag{12}$$

The time shift (denoted by subscript 'shft') representing the difference in propagation time (t_{prop}) associated with the change in sound speed Δc, can be seen to vary with the propagation distance, s, according to

$$t_{\text{shft}} = t_{\text{prop}(0)} - t_{\text{prop}(i)} = \frac{s}{c_0} - \frac{s}{c_0+\Delta c}. \tag{13}$$

This rearranges to

$$t_{\text{shft}} = \frac{s\Delta c}{c_0(c_0+\Delta c)}, \tag{14}$$

which for $\Delta c \ll c_0$ is equivalent to

$$t_{\text{shft}} = \frac{s\Delta c}{c_0^2}, \tag{15}$$

where similarly to Eq. (4),

$$t_{\text{obs}} = t_{\text{src}} + t_{\text{shft}}. \tag{16}$$

In this case, the propagation distance is the average displacement of the piston from the survey bin. s is therefore a function of the piston extension and the spacing '$\mathscr{B}$' from the fully extended piston to the survey bin, namely,

$$s = \frac{Mc_0}{\omega} + \mathcal{B}. \tag{17}$$

Combining Eqs. (12), (15) and (17), substituting into Eq. (16), and then into Eq. (8), the curve reduces to

$$\mathcal{W} = \sin\left(\omega t_{\text{src}} + \left(M+\frac{\mathcal{B}\omega}{c_0}\right)\left(\sqrt{1+\frac{rM}{T_0}}-1\right)\sin(\omega t_{\text{src}})\right). \tag{18}$$

This result again validates the construction of Eq. (1), but also indicates that the minor frequency dependence seen in Fig. 13 stems from the fixed width of the buffer region between the extended piston and the survey bin, which can also be seen through the stratification of the contours in Fig. 14. As the role of the buffer region is purely for data acquisition and is not illustrative of the source itself, the more accurate representation of the source steepening should be of the form

$$\mathcal{W} = \sin\left(\omega t_{\text{src}} + M\left(\sqrt{1+\frac{rM}{T_0}}-1\right)\sin(\omega t_{\text{src}})\right), \tag{19}$$

which is the developed oscillatory function with χ as a function of M, T_0 and r. Furthermore, the frequency dependence of the data should be neglected during parameterisation, since it is not caused by the

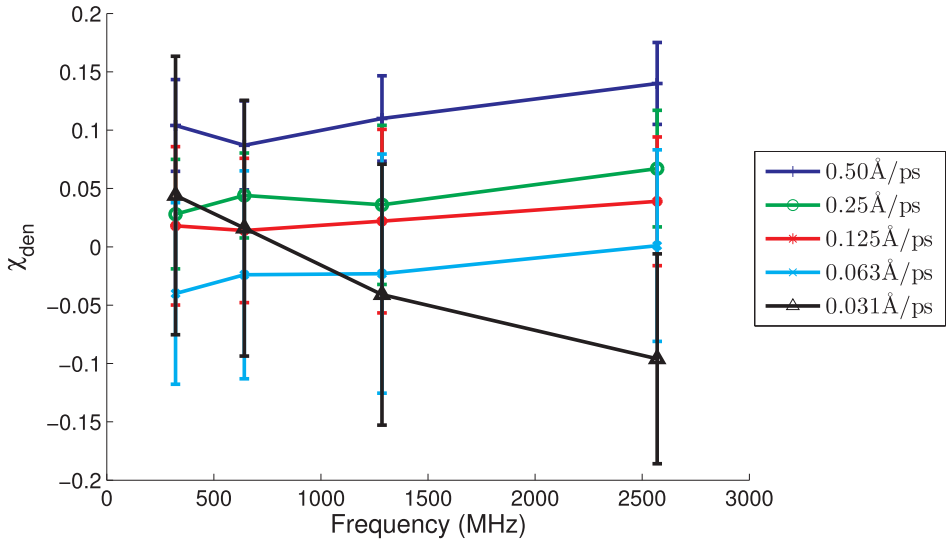

Fig. 18. The steepening term of the density curve, χ_{den}, with error bars of two standard errors, as a function of frequency for different source amplitudes. (Colour available online).

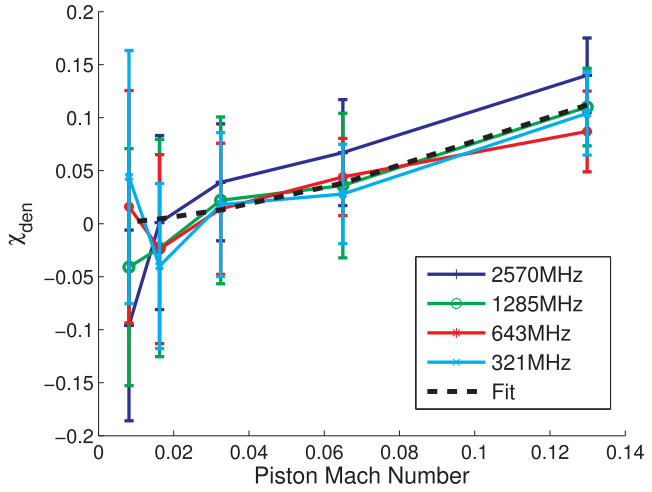

Fig. 19. The steepening term of the density curve, χ_{den}, with error bars of two standard errors, as a function of the normalised source velocity amplitude (Mach number) for different frequencies. A curve of best fit using Eq. (3) also applied. (Colour available online).

Table 1
Width and steepening term parameterisation for velocity and density using Eq. (1); $O(\omega, \psi, \chi) = A\sin(\omega t + \psi\sin^2(\frac{\omega t}{2}) + \chi\sin(\omega t))$.

	Width Term, ψ	Steepening Term, χ	
	Slope Coefficient, m	Amplitude Coefficient, n	Exponent, p
Velocity	2.25	1.08	1.33
Density	3.53	2.65	1.55

source. This will reduce the contribution from the buffer region, but it will be impossible to entirely remove the influence of the buffer region given the data obtained. Comparing Eqs. (18) and (1) indicates that χ is a function of M with components of order 1 and 1.5. Thus it is reasonable to expect that the single term approximation (Eq. (3)) has an exponent, p, between 1 and 1.5. As the width modification and steepening occur concurrently and independently, we can consider the two time transformations to act together to result in the novel oscillatory curve given by Eq. (1).

4.2.3. Velocity parameterisation

Using Eq. (2), the parameterised linear fit for the velocity width term, ψ_{vel}, the slope coefficient m was found to be 2.25, and is shown in Fig. 12. This value is relatively consistent with the theoretical value of 2 derived in Section 4.2.2, which fits within the envelope of the error bars except at the highest velocity, where the overlap of the error bars for different frequencies is limited. The discrepancy of 0.25 could be due to another phenomenon causing widening, but it is apparent that the pseudo-Doppler effect is the main contributor to the width modification.

Applying Eq. (3), the higher order parameterisation for the velocity steepening term χ_{vel} was found to have best fit amplitude coefficient, n, of 1.08 and exponent, p, of 1.33, and is shown in Fig. 14. Though the parameterisation could be more accurate, and more consistent with the analysis in Section 4.2.2, adding more terms to the fitting curve would add undesired complexity.

4.3. Density wave

Due to the different boundary condition that applies for the gas density, the assumptions made about the region directly adjacent to the piston cannot be imported from the velocity discussion. The formation of the density wave is affected by the density of the region at the moment immediately prior and the contribution from any reflected wave component, rather than simply matching the instantaneous motion of the piston. Since the formation of the density wave affects the piston force and the propagating wave experiences the same phenomena as the velocity wave, the earlier analysis can assist with understanding the distortion of the shape of the density wave.

4.3.1. Density data

The width term of the density wave displays similar features to that seen for the velocity wave. Fig. 16 also shows a slight decreasing slope for the 0.5 Å/ps curve. A strong dependence on the source Mach number is demonstrated in Fig. 17. This is consistent with the dependence identified for the force and velocity.

Fig. 18 illustrates that the steepening of the density curve is not strongly frequency dependent due to the curves being relatively flat. This agrees with Fig. 19, in which the stratification of the curves is limited, despite the frequencies differing by as much as a factor of 8. The size of the error bars at the lowest Mach number plotted in Fig. 19 indicates that the signal-to-noise ratio for the density data at such a low source amplitude is insufficient to give reliable results for the number of

periods averaged. Excluding these points, the density wave shows a similar higher order curve to the velocity wave (see Fig. 19). It is of note that exclusion of these points does not inherently extend to the same force and velocity results, as the underlying noise for these signals is not the same.

4.3.2. Density analysis

Since the density data was collected from the stationary survey bin, the density wave derived will be subject to the same pseudo-Doppler effect discussed in Section 4.2.2. The width terms, however, are not equal to those of the equivalent velocity cases as the density is also influenced by other effects. The force curve possesses a width term due to the density at the piston, among other factors, varying nonlinearly with the motion of the piston. As such, the density curve to which the Doppler effect is applied is not a perfect sinusoid prior to the Doppler shift. Hence, the resultant density waveshape is more distorted than the velocity waveshape.

Similarly, steepening via the same mechanisms described for the velocity wave occurs for the density wave, though the values for curve terms in the density case are consistently greater than in the velocity case. This is consistent with the addition of steepening due to the pseudo-Doppler effect and propagational steepening to the distortion of the shape of the force curve, which is influenced by the density at the face of the source.

However, the width and steepening terms formed by the pseudo-Doppler effect and propagational steepening are characteristic of a time transformation, but the distortion to the wave that occurs during the wave formation at the piston surface is not. As such, the terms from the velocity wave, though caused by the pseudo-Doppler effect and propagational steepening, cannot be linearly combined with the force terms to produce the density terms. In fact, a time transformation applied to the novel oscillatory function would result in nested sinusoids within the nested sinusoids, which exceeds the simplicity desired for the parameterised approximations.

4.3.3. Density parameterisation

Consistent with the velocity wave data, the width term for the density wave appears to be linear, while the steepening term has a higher order curve. The parameterised linear fit for the density width term, ψ_{den}, yielded a slope coefficient m of 3.53 (see Fig. 17). Though the width terms from the force and velocity cannot be linearly summed to determine the density width term, the force slope approximating 1.85 and the velocity slope of 2.25 does correspond to the order of magnitude of the slope coefficient determined for the density width term.

The higher order curve for the density steepening term χ_{den} is shown to have an amplitude coefficient, n, of 2.65 and exponent, p, of 1.55 (see Fig. 19).

As suggested in Section 4.3.2, the values obtained for the density parameterisation exceed those found for the velocity parameterisation, as the density experiences both the memory effects demonstrated in the force analysis and the pseudo-Doppler effects discussed for the velocity wave, as demonstrated by Table 1.

5. Conclusion

Distortion of the acoustic wave has been demonstrated to occur at the source at high frequency combined with a non-negligible Mach number source amplitude. The modified equation for the oscillatory curve (Eq. (1)) is seen to be robust, constructed to be consistent with the underlying causes of the widening and steepening observed for the wave, and assists with the analysis of the data. Analysis concludes that the development of this distortion is due to a density memory effect and a psuedo-Doppler effect that is noticeable when the source velocity amplitude is more than a few percent of the sound speed.

A set of equations that characterise the non-sinusoidal waveshape created by a sinusoidally oscillating source were developed. The values obtained from parameterisations were found to be strongly dependent on the Mach number of the source and independent of the frequency. Table 1 shows the parameterised width terms which are seen to be linearly dependent on the Mach number, and the steepening terms are shown to have a power relationship with the Mach number.

In practical applications the improved understanding of the nuances of high frequency acoustic waveshapes may assist with improving the fidelity of parametric acoustic arrays. The developed parameterisation equations and values can be used to produce an analytical formulation of an acoustic source that uses mass and velocity manipulation instead of an oscillating plane, when a sinusoidally oscillating infinite impedance source is being modelled. The equations can also be transferred to other types of models to act as a set of boundary conditions equivalent to a high-frequency acoustic source. This is most suitable for models for which using a moving boundary is impractical. In particular, a more thorough description of the sound source may, when combined with existing acoustic theory, facilitate the construction of a truncated MD domain model that is not inhibited by the domain length constraints discussed in Section S1 of the supplementary material document. Though it is likely that such a truncated MD domain would only be suitable when forming part of a greater hybrid model, such a system would have a significantly lower computational cost than a system using a longer MD domain.

Acknowledgements

This research was supported by the Australian Research Council's Discovery Projects funding scheme (project number DP 130102832).

Appendix A. Supplementary material

Supplementary data associated with this article can be found, in the online version, at https://doi.org/10.1016/j.ultras.2019.02.001.

References

[1] L. Desvillettes, S. Lorenzani, Sound wave resonances in micro-electro-mechanical systems devices vibrating at high frequencies according to the kinetic theory of gases, Phys. Fluids 24 (9) (2012) 092001.
[2] N.G. Hadjiconstantinou, A.L. Garcia, Molecular simulations of sound wave propagation in simple gases, Phys. Fluids 13 (4) (2001) 1040–1046.
[3] K. Aoki, S. Kosuge, T. Fujiwara, T. Goudon, Unsteady motion of a slightly rarefied gas caused by a plate oscillating in its normal direction, Phys. Rev. Fluids 2 (1) (2017) 013402.
[4] M.P. Allen, D.J. Tildesley, Computer Simulation of Liquids, Oxford University Press, 1989.
[5] P.J. Westervelt, Parametric acoustic array, J. Acoust. Soc. Am. 35 (4) (1963) 535–537.
[6] M. Ayub, Experimental and numerical investigation of a carbon nanotube acoustic absorber, PhD Thesis University of Adelaide, 2015.
[7] H. Bennett, A. Zander, B. Cazzolato, D. Huang, Speedup techniques for molecular dynamics simulations of the interaction of acoustic waves and nanomaterials, 21st International Congress on Modelling and Simulation, vol. 21, Modelling and Simulation Society of Australia and New Zealand, 2015.
[8] T. Yano, Molecular dynamics study of sound propagation in a gas, AIP Conference Proceedings, vol. 1474, AIP, 2012, pp. 75–78.
[9] M. Ayub, A. Zander, C. Howard, B. Cazzolato, D. Huang, A review of md simulations of acoustic absorption mechanisms at the nanoscale, Proc. Acoust. 2013 (2013) 17–20.
[10] O. Rudenko, S. Soluyan, Theoretical Foundations of Nonlinear Acoustics, Consultants Bureau, 1977.
[11] M. Ayub, A. Zander, D. Huang, B. Cazzolato, C. Howard, Molecular dynamics simulations of classical sound absorption in a monatomic gas, J. Sound Vib. 421 (2018) 319–333.
[12] S. Plimpton, Fast parallel algorithms for short-range molecular dynamics, J. Comput. Phys. 117 (1) (1995) 1–19.
[13] J.D. Weeks, D. Chandler, H.C. Andersen, Role of repulsive forces in determining the equilibrium structure of simple liquids, J. Chem. Phys. 54 (12) (1971) 5237–5247.
[14] F.F. Abraham, Y. Singh, The structure of a hard-sphere fluid in contact with a soft repulsive wall, J. Chem. Phys. 67 (5) (1977) 2384–2385.
[15] R. Dorf, The Engineering Handbook, second ed., Electrical Engineering Handbook, CRC Press, 2004.